

# TDC Sharing in SPAD-Based Direct Time-of-Flight 3D Imaging Applications

Foad Arvani, Tony Chan Carusone, The Edward S. Rogers Sr. Department of Electrical & Computer Engineering (ECE), University of Toronto, Toronto, Canada, Email: foad.arvani@isl.utoronto.ca

**Abstract**—TDC specifications are critical determinants of the range, resolution, and accuracy of SPAD-based TCSPC 3D imaging systems. In particular, the TDC conversion time plays a vital role in emerging architectures wherein TDCs are shared across the sensor array. Here, a statistical analytical model is employed to relate the number of required TDCs per SPAD array to the 3D image accuracy and frame rate, taking into account environmental factors such as ambient light and distance. The model verifies that sharing schemes, contrary to TDC-per-SPAD scheme, can improve efficient use of area and power, and it also permits TDC sharing architectural exploration to determine the number of TDCs required for given array size. Monte Carlo numerical simulations verify the accuracy of the proposed method.

**Keywords**—Time-to-digital converter (TDC), time-of-flight (ToF), time-correlated single photon counting (TCSPC), LiDAR, single photon avalanche diode (SPAD), dead time, inhomogeneous continuous-time Markov chain (ICTMC), Monte Carlo, Data Converter, jitter

## I. INTRODUCTION

Emergent applications in engineering, science, and entertainment are driving the three-dimensional (3D) sensor market growth [1-3]. This expansion includes a rising demand for 3D-enabled light detection and ranging (LiDAR) modules in autonomous vehicles, medical imaging systems, and consumer electronics. There have been various methods presented in the literature to address this need [2]. However, SPAD-based direct time-of-flight (D-ToF) active optical range measurement seems to be the most promising for mobile applications as it provides better accuracy, range, and reliability in compact, low power systems [1].

SPADs require quenching circuitry for proper operation [4], and saturate when more than one photon reaches the detector during the same measurement time slot. The so-called “pile-up” distortion effect increases the measurement time required to achieve a desired dynamic range (DR) [5]. To cope with the latter, a macro pixel comprising an array of small SPAD cells may be beneficial which can demonstrate a high dynamic range (DR) exceeding 110 dB [5]. The macro pixel is called a digital silicon photomultiplier (dSiPM). Meanwhile, the number of time-to-digital-converters (TDC) allocated for processing of the arrival time of multiple pulses generated by a sensor array or dSiPMs is a question yet to be addressed. Upcoming complex TDC sharing schemes necessitate extensive simulations to clarify the tradeoffs in the system design [6]. Also, the simulation time and accuracy should be acceptable to reflect the design parameters sweep effects efficiently.

Conventionally, Monte Carlo simulations are run to fulfill

this purpose which includes generating SPAD trigger sequences, multiplexing the arrivals from SPADs, and finally, arrival time processing to create the histogram. Although these simulations generate realistic samples of the system, their accuracy depends on the computation time which increases dramatically with the sensor array size. On the other hand, in analytical simulation, results are created almost instantly, parametrization helps to develop design insight, and as a result, it facilitates parametric sweeps of design variables.

Most analytical methods suffer from limited accuracy or are valid only under certain assumptions [7]. The authors in [8] have introduced an analytical model to overcome these limitations by incorporating the time-inhomogeneous nature of the received pulses including the dead time of TDCs (i.e. when they are busy digitizing a pulse and therefore unavailable). This work uses the analytical model of [8] to clarify the required number of TDCs in D-ToF time-correlated single photon counting (TCSPC) systems by relating the system performance to the number of TDCs under realistic environmental conditions.

In section II, an analytical methodology to analyze the TCSPC time-of-arrival histograms is presented. Section III relates the number of TDCs per SPAD array to D-ToF ranging performance metric accompanied by the simulation results and discussion.

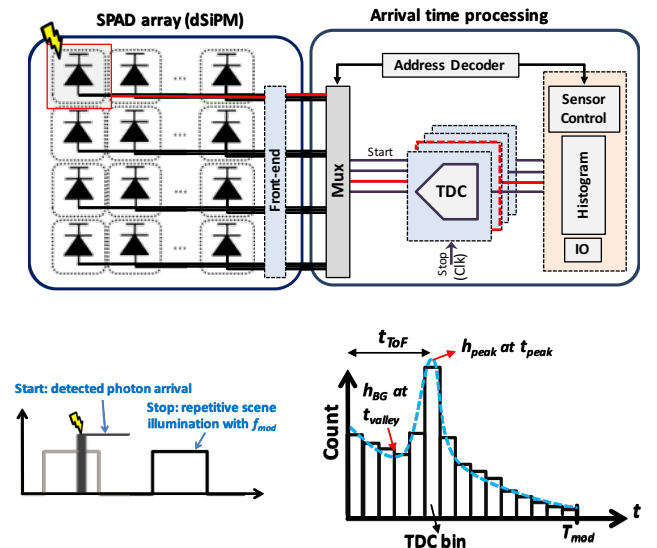


Fig. 1. Top: the direct ToF TCSPC system block diagram with TDC sharing scheme: the assigned TDCs extract the timing of the detected photon arrivals; bottom left: the repetitive scene probing with  $f_{mod}$  and a noisy time-stamped photon arrival; bottom right: the reconstructed time-of-flight histogram

## II. TERMINOLOGY AND METHODS

In the TCSPC system, the output of the SPAD array is a sequence of pulses coinciding with the first photon arrivals within each repetition period  $T_{mod}$ , including some false triggers generated by background illumination or dark counts. TDCs measure the pulse arrival times relative to synchronizing ‘‘Stop’’ pulses, and a histogram of arrival times is created over many detections, providing the basis for calculating the time-of-flight. Typically, the SPAD activity rate is low (less than one photon detected per multiple repetition illumination pulses) in TCSPC systems [2]. Hence, TDCs can be shared among several SPADs (versus the common TDC-per-SPAD configuration), thus reducing circuit area and power consumption. However, depending on the processing time of the TDCs and the number of available TDCs, there may be some missed pulses. For example, assuming a dSiPM comprising 8 SPADs and 2 TDCs with a dead time of 10ns to process the arrivals from all the SPADs, Fig. 2 illustrates the time-inhomogeneous behavior of photon detection. In this example, three photon arrivals are missed and not detected as all TDCs are busy, two of which corresponds to the reflected light from the target while one is because of the background light. Missed counts decrease the contrast in the histogram, and increase variance of the measured distance. In this section, the analytical model introduced in [8] will be further investigated and then used to establish the relation between the number of TDCs per SPAD array, and the D-ToF ranging performance metric.

### A. System Description: Analytical Histogram

Incorporating the TDC dead time effects in the time-inhomogeneous TCSPC system with TDC LSB (or equivalently the histogram bin width) of  $\Delta t$ , TDC dead time of  $\tau_{dead}$ , and  $N = T_{measurement} / T_{mod}$  representing the number of scene probing repetitions (acquisitions), [8] estimates the effective photon arrival rate  $R_{eff}$ . For the reflected light photon arrival rate of  $\lambda_{sig}(t) = P_{sig}(t)/E_{photon} \cdot \eta_{PDE}$ , and background light photon arrival rate of  $\lambda_{BG} = P_{BG}/E_{photon} \cdot \eta_{PDE}$  with  $\eta_{PDE}$  denoting the SPAD photon detection efficiency, the blocking probability  $p_n(t)$  that all  $n$  TDCs are busy at time  $t$  is [8]

$$p_n(t) = \frac{\frac{(\overline{R(t)} \cdot \tau_{dead})^n}{n!}}{\sum_{j=0}^n \frac{(\overline{R(t)} \cdot \tau_{dead})^j}{j!}}$$

where  $R(t)$  is the total first photon arrival rate, and  $R_{eff}$  takes missed counts into account:

$$R(t) = (\lambda_{BG} + \lambda_{sig}(t)) \cdot \exp\left\{-\int_0^t (\lambda_{BG} + \lambda_{sig}(u)) du\right\}$$

$$R_{eff}(t) = R(t) \cdot [1 - p_n(t)]$$

and  $\overline{R(t)} = \frac{1}{\Delta t} \int_t^{t+\Delta t} R(u) du$  denotes the average arrival rate in  $[t, t + \Delta t]$ .

Then authors in [8] assess the corresponding analytical ToF histogram  $h(\tau)$ ,  $\tau \in [0, \Delta t, 2\Delta t, \dots, (\frac{T_{mod}}{\Delta t} - 1)\Delta t]$

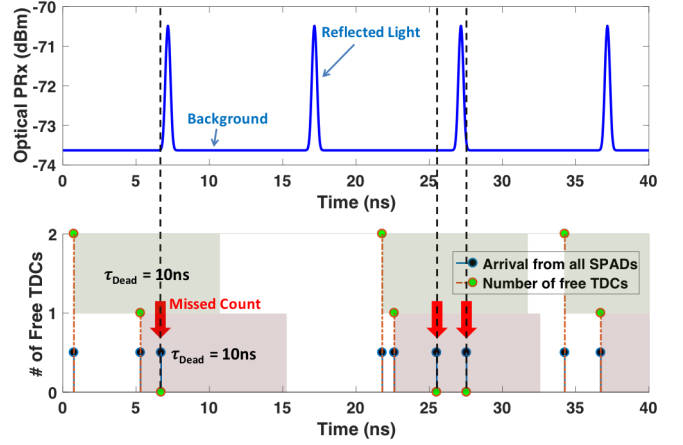


Fig. 2. Time-inhomogeneous photon arrival; top: the reflected pulses at the receiver with  $f_{mod} = 100\text{MHz}$ , bottom: two TDCs with dead time of 10ns time-stamp the arrivals comprising the multiplexed arrivals from 8 SPADs resulting in three missed counts

$$h(\tau) = N \int_{\tau - \frac{\Delta t}{2}}^{\tau + \frac{\Delta t}{2}} R_{eff}(t) dt \approx R_{eff}(\tau) \cdot \Delta t \cdot N$$

### B. Effective $\tau_{Dead}$

The mean time between two photon arrivals is the inverse of the arrival rate [9]. So, examining the relation between the arrival rate and the effective arrival rate provides a means to assess the efficiency of TDC sharing scheme by calculating the effective dead time  $\tau_{eff}$

$$\frac{1}{R_{eff}} = \frac{1}{R} + \tau_{eff}$$

Assuming  $n$  is the number of the shared TDCs and  $\overline{R(t)}$  is the average multiplexed arrival rate from all SPADs, the effective dead time  $\tau_{eff}$  is always shorter than the effective non-shared value  $\tau_{dead}/n$

$$\tau_{eff} = \frac{\tau_{dead}}{n} \cdot \frac{\frac{(\overline{R(t)} \cdot \tau_{dead})^{n-1}}{(n-1)!}}{\sum_{j=0}^{n-1} \frac{(\overline{R(t)} \cdot \tau_{dead})^j}{j!}} = \frac{\tau_{dead}}{n} \cdot p_{n-1} < \frac{\tau_{dead}}{n}$$

The efficiency of sharing scheme depends on  $\overline{R(t)} \cdot \tau_{dead}$  meaning that systems with low arrival rate such as TCSPC, and consequently smaller  $p_{n-1}$  (probability of  $n-1$  busy TDCs at time  $t$ ), will benefit more from sharing schemes. This conclusion shows the importance of TDC sharing schemes to achieve low power and high throughput TCSPC systems.

### C. D-ToF Ranging Performance Metrics: SNR and $Q$

The common performance metrics in laser-based distance measurements are the signal-to-noise ratio (SNR) and  $Q$  [10]

$$SNR \stackrel{\text{def}}{=} \frac{h_{peak}}{\sqrt{h_{peak} + h_{BG}}} = \sqrt{h_{peak}} \cdot \sqrt{\frac{SBR}{1 + SBR}}$$

$$Q \stackrel{\text{def}}{=} \frac{h_{peak} - h_{BG}}{\sqrt{h_{peak}} + \sqrt{h_{BG}}}$$

where  $SBR = h_{peak} / h_{BG}$ , and  $h_{peak}$  and  $h_{BG}$  represent the counts at the peak of the histogram and the counts at the valley caused by the background light (refer to Fig 1). To determine the  $SNR$  and  $Q$  for a given measurement condition and system setup,  $t_{peak}$ , and  $t_{valley}$  can be spotted by  $\partial h(\tau) / \partial \tau = \frac{\partial h}{\partial R} \cdot \frac{\partial R}{\partial \tau} = 0$ .

While  $\partial R / \partial \tau$  is a function of  $P_{Rx}$ , system jitter  $\sigma$ , and whatever defines the shape of  $R(t)$ ,  $\partial h / \partial R$  is a function of  $n$  (the number of available TDCs), the dead time  $\tau_{dead}$ , and whatever that causes blocking and missed counts. The typical diffusion tail present in SPAD timing responses often submerge under the background level of the TCSPC histogram [11], so for the case of a Gaussian illumination pulse, the power distribution of the reflected pulse at the detector  $P(t)$  is

$$P(t) = \frac{P_{Rx}}{\sqrt{2\pi}\sigma f_{mod}} \exp\left(-\frac{(t - t_{ToF})^2}{2\sigma^2}\right) + P_{BG}$$

With  $E_{photon}$  representing the energy of a photon and  $N_{Monte}$  the number of Monte Carlo simulations, we have

$$\begin{aligned} \frac{\partial R}{\partial \tau} &= \frac{P_{Rx}\eta_{PDE}}{\sqrt{2\pi}\sigma E_{photon}f_{mod}} e^{-\left(\frac{\tau - t_{ToF}}{2\sigma^2}\right)^2} \\ &\cdot \left\{ \frac{\tau - t_{ToF}}{\sigma^2} + \frac{P_{Rx}\eta_{PDE}}{\sqrt{2\pi}\sigma E_{photon}f_{mod}} e^{-\left(\frac{\tau - t_{ToF}}{2\sigma^2}\right)^2} \right. \\ &\quad \left. + 2\lambda_{BG} \right\} + \lambda_{BG}^2 \\ \frac{\partial h}{\partial R} &= \Delta\tau \cdot N_{Monte} \cdot (1 - p_n \cdot (n + 1 - \mu)) \end{aligned}$$

where  $\mu$  is the expected value of the number of busy TDCs. For high illumination operation where  $\overline{R(t)} \cdot \tau_{dead} \gg 0.1$ ,  $\mu$  tends to  $np_n$ , meaning that all the TDCs are busy all the time, and as the system will experience high blockage,  $\mu$  goes to  $n$ . On the other hand, for low light operation where  $\overline{R(t)} \cdot \tau_{dead} \ll 0.1$ ,  $\mu$  tends to zero. The latter case is equivalent to a high number of TDCs available to handle the incoming arrivals, and essentially zero dead time for the system. As a result, the term  $\partial h / \partial R$  gives no zeros for  $\partial h / \partial \tau = 0$  and so does not contribute to the position of the  $t_{peak}$  and  $t_{valley}$ . Therefore,  $\partial R / \partial \tau = 0$  determines the position of the extremum points  $t_{peak}$  and  $t_{valley}$ . Under no background noise condition,  $\partial R / \partial \tau = 0$  simplifies to

$$\frac{\tau - t_{ToF}}{\sigma^2} + \frac{P_{Rx}\eta_{PDE}}{\sqrt{2\pi}\sigma E_{ph}f_{mod}} e^{-\left(\frac{\tau - t_{ToF}}{2\sigma^2}\right)^2} = 0$$

which is consistent with the results provided in [8].

### III. THE NUMBER OF TDCS PER SPAD ARRAY AND $SNR$

As different algorithms require different levels of  $SNR$  in the histogram to guarantee for a given performance regarding the accuracy and precision of the measured distance, the focus is to determine how the  $SNR$  and  $Q$  change with the number of TDCs. First, the environmental conditions for an example application of indoor 3D imaging are introduced. Then, the analytical model will be employed to study the  $SNR$  of the histogram versus the number of TDCs per SPAD array, and distance.

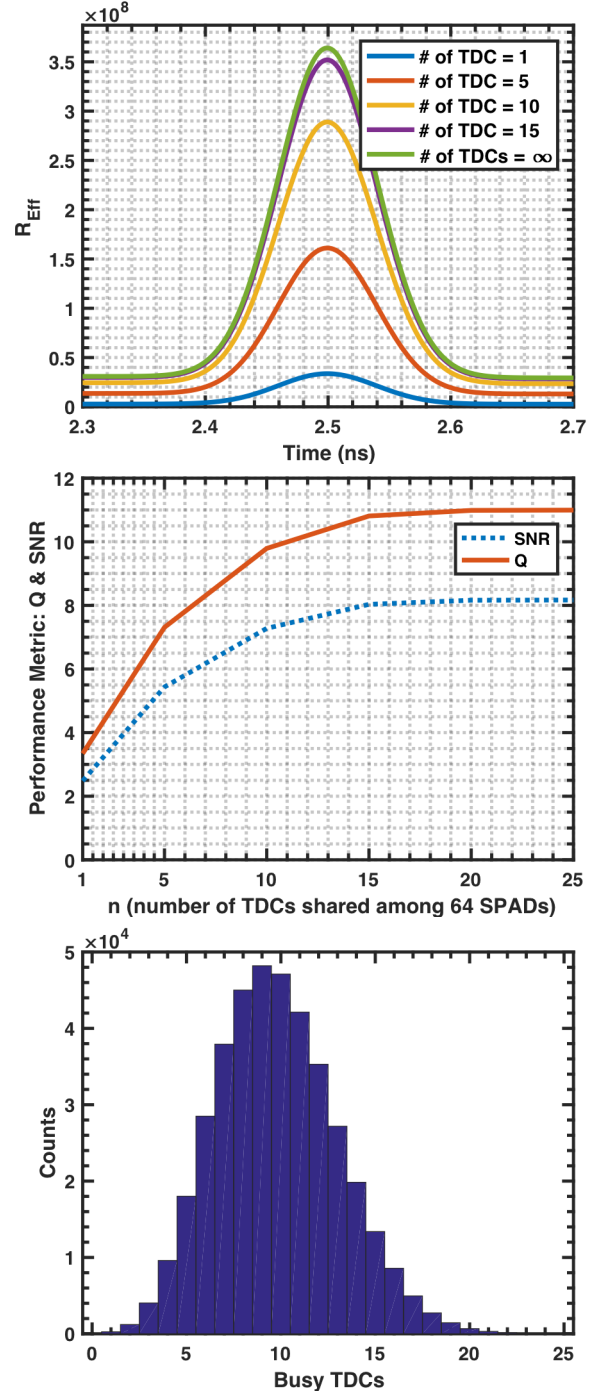


Fig. 3. Performance metrics for the TDCs-per-cluster sharing scheme for a target at a distance of  $t_{ToF} = 2.5$ ns; top: effective arrival rate  $R_{eff}$  for different number of TDCs; middle:  $SNR$  and  $Q$  versus  $n$  (the number of TDCs), bottom: numerical histogram of the number of busy TDCs confirms that increasing the number of TDCs per SPAD array beyond 15 has no significant effect under this measurement condition

#### A. Indoor Measurement Conditions

A typical indoor security application requires about 2mm of depth resolution and a range of about 1m. Table 1 summarizes the corresponding simulation parameters. The proposed methodology can be applied to any TCSPC environmental conditions.

TABLE I. SUMMARY OF THE MEASUREMENT CONDITIONS OF THE EXAMPLE INDOOR APPLICATION

Parameters	
SPAD	size 8×8, jitter $FWHM = 15$ ps
Laser	Tx average power = 50mW, pulse $FWHM = 0.1$ ns, $f_{mod} = 100$ MHz
Ambient light	Unfiltered 300lux ( $\lambda_{BG} \approx 33$ MHz)
Default values	$n = 15$ (the number of TDCs per SPAD array), TDC $\tau_{dead} = 5$ ns, TDC $LSB$ width = 10ps, $\sigma_{TDC} = 10$ ps, distance = 30cm

### B. SNR vs. the Number of TDCs per SPAD Array in TDCs-per-Cluster Sharing Scheme

As shown earlier, the probability of blockage  $p_n$  and the missed counts depends on the incoming arrival rate, the array size, the system dead time, and the number of TDCs assigned to process the incoming multiplexed detections. Assigning more TDCs to process the sequence can reduce the effective dead time of the total system, and hence, the missed counts. However, increasing the number of TDCs, increases the power consumption and degrades the fill factor of the sensor.

Besides, increasing the number of TDCs will not improve the performance beyond some point, while it consumes more power and area. Fig. 3 shows the effective arrival rate  $R_{Eff}$ ,  $SNR$ , and  $Q$  of the reconstructed histogram versus the number of TDCs per SPAD array in TDCs-per-cluster sharing scheme for an array consisting of 8×8 SPADs. It shows that for this measurement setup, the required  $SNR$  for a specific algorithm will map to the minimum required number of TDCs to handle the multiplexed incoming arrival sequence. In this case, with  $n = 15$  TDCs, 95% of the maximum attainable  $SNR$  is achieved. This limit is also verified with numerical Monte Carlo simulation shown at the bottom of Fig. 3 which confirms that increasing the number of TDCs beyond 15 has no significant effect since very few arrivals would be time-stamped by TDCs #16 onward.

### C. SNR vs. Distance or Equivalently Time-of-Flight

When the distance to the target increases, the optical power at the receiver drops. As a result, the arrival rate reduces, and consequently, the  $SNR$  degrades. Also, as the time-of-flight increases, the probability of false SPAD trigger rises, leading to more incorrect time-stamping. Fig. 4 shows the effective arrival rate  $R_{Eff}$ ,  $SNR$ , and  $Q$  of the reconstructed histogram versus the target distance or equivalently time-of-flight.

### CONCLUSIONS

This paper employs a statistical analytical model which enables the investigation of the TDC sharing schemes by relating the number of required TDCs to the  $SNR$  performance metric, considering environmental factors such as ambient light and distance. Our analysis provides a direct and intuitive approach to study the system and to quantify the effects of the TDC sharing on the system performance. The results, which lead to the necessary insight into the behaviour of the TDC sharing schemes, are validated by numerical Monte Carlo simulations.

For the exemplary indoor low-cost application and the corresponding typical specifications of lasers and detectors, the

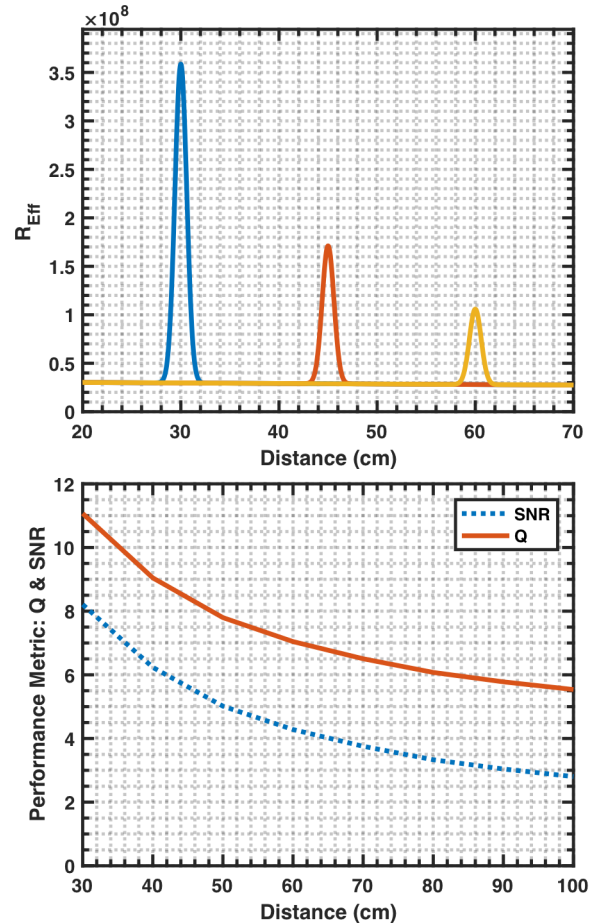


Fig. 4. Performance metrics for the TDCs-per-cluster sharing scheme with  $n = 15$  (the number of shared TDCs); top: effective arrival rate  $R_{Eff}$  versus the target distance (or equivalently  $t_{ToF}$ ), bottom:  $SNR$  and  $Q$  versus the target distance

introduced method indicates that 15 TDCs are appropriate for an 8×8 array of SPAD detectors which can lead to over 75% less power consumption compared to TDC-per-SPAD scheme.

### REFERENCES

- [1] P. Cambou and G. Girardin, "3D Imaging and Sensing: From Technologies to Market," Yole Développement 2018.
- [2] F. Remondino and D. Stoppa, *TOF range-imaging cameras*. Springer, 2013, pp. 1-240.
- [3] A. Süß, *High Performance CMOS Range Imaging: Device Technology and Systems Considerations*. CRC Press, 2016.
- [4] A. Gallivanoni, I. Rech, and M. Ghioni, "Progress in Quenching Circuits for Single Photon Avalanche Diodes," *IEEE Transactions on Nuclear Science*, vol. 57, no. 6, pp. 3815-3826, 2010.
- [5] S. Gnechi *et al.*, "Analysis of Photon Detection Efficiency and Dynamic Range in SPAD-Based Visible Light Receivers," *Journal of Lightwave Technology*, vol. 34, no. 11, pp. 2774-2781, 2016.
- [6] M. A. Tetrault, A. C. Therrien, W. Lemaire, R. Fontaine, and J. F. Pratte, "TDC Array Trade-Offs in Current and Upcoming Digital SiPM Detectors for Time-of-Flight PET," *IEEE Transactions on Nuclear Science*, vol. PP, no. 99, pp. 1-1, 2017.
- [7] M. Beer, O. M. Schrey, B. J. Hosticka, and R. Kokozinski, "Expected Value and Variance of the Indirect Time-of-Flight Measurement With Dead Time Afflicted Single-Photon Avalanche Diodes," *IEEE Transactions on Circuits and Systems I: Regular Papers*, vol. 65, no. 3, pp. 970-981, 2018.

- [8] F. Arvani and T. C. Carusone, "Direct Time-of-Flight TCSPC Analytical Modeling Including Dead-Time Effects," in *2018 IEEE International Symposium on Circuits and Systems (ISCAS)*, 2018, pp. 1-4.
- [9] S. M. Ross, *Introduction to Probability Models: Eleventh Edition*. 2014, pp. 1-767.
- [10] P. Sara, S. B. Gerald, M. S. Jason, M. W. Andrew, and C. Sergio, "Laser-based distance measurement using picosecond resolution time-correlated single-photon counting," *Measurement Science and Technology*, vol. 11, no. 6, p. 712, 2000.
- [11] M. J. D. Darek P. Palubiak, "CMOS SPADs: Design Issues and Research Challenges for Detectors, Circuits, and Arrays," *IEEE Journal of Solid-State Circuits*, vol. 20, no. 6, 2014.